PNAS RESEARCH ARTICLE | EARTH, ATMOSPHERIC, AND PLANETARY SCIENCES OPEN ACCESS

Concomitant formation of protocells and prebiotic compounds under a plausible early Earth atmosphere

Christian Jenewein[a], Aurora Maíz-Sicilia[b], Fernando Rull[c], Lorena González-Souto[d], and Juan Manuel García-Ruiz[a,b,1]

Affiliations are included on p. 7.

Edited by Alexandra Navrotsky, Arizona State University, Tempe, AZ; received July 10, 2024; accepted November 20, 2024

Revealing the origin of life and unambiguously detecting fossil remains of the earliest organisms are closely related aspects of the same scientific research. The synthesis of prebiotic molecular building blocks of life and the first compartmentalization into protocells have been considered two events apart in time, space, or both. We conducted lightning experiments in borosilicate reactors filled with a mixture of gases mimicking plausible geochemical conditions of early Earth. In addition to the variety of prebiotic organic molecules synthesized in these experiments, we investigated the micrometer-thick silica-induced organic film that covers the walls of the reactors and floats at the water–gas interface. We found that the film is formed by aggregation of HCN-polymer nanoclusters whenever water is present, either in the liquid or vapor phase. The organic film morphs into micrometer-scale biomorphic vesicular structures hanging from the organic film into the water. We also show that these structures are hollow and may act as microreactors facilitating chemical pathways toward increasing complexity. We propose that these organic biomorphs form through a bubble-driven mechanism and interfacial precipitation of HCN-polymers. The concomitant synthesis of biomorphic poly-HCN protocells and prebiotic molecules under plausible geochemical conditions of early Earth-like planets and moons and opens a different geochemical scenario for the emergence of life. Our results suggest that the coexistence of molecular building blocks of life and submicron biomorphic structures in the oldest rocks on Earth or any other celestial body does not necessarily mean evidence of life.

origin of life | Miller experiment | silica | prebiotic chemistry | protocells

Significance

Miller–Urey experiments demonstrated that prebiotic organic compounds can be synthesized from a reducing atmosphere, alkaline water, and electrical discharges. We show that in these experiments, only in the presence of water, silica induces the formation of a solid organic film made of polymers of hydrogen cyanide. In these films, we found nano- to micron-size biomorphic protocells forming through a mechanism of bubbling and water–gas interfacial precipitation. Our results suggest that protocells and the key molecules of life already coexisted on the earliest Earth, setting stage for the emergence of life and additional criteria for life detection. These organic "protoworlds" could be widely distributed across the universe on any Earth-like body where they might follow different evolutionary paths.

Cellular organization is a key characteristic of life as we know it. Living organisms are made of cells, i.e., tiny, self-contained, self-regulated units surrounded by a membrane that allows the transfer of mass and energy with their neighbors and the surrounding environment (1–3). Although liquid–liquid demixing could lead to membraneless coacervates and proteinoids (4), it is difficult to conceive that life as we know it could be a boundless cluster of chemicals. Therefore, it is thought that an unavoidable step in the pathway from inanimate matter to life is the compartmentalization of space into hollow structures that act as chemical microreactors, leading to compounds of increasing complexity (5–7). This is why the protocols for detecting the earliest signature of life often seek hollow structures of biological shapes that could be the remnants of the oldest, most primitive living beings (8–10).

Several mechanisms of formation of organic, mineral, or mineral-organic membranes could account for the simpler processes of compartmentalization and thus encapsulating organic compounds. Vesicles have been experimentally shown to form from nonphospholipids, amphiphiles, and lipids (5, 11, 12). Encapsulation of prebiotic molecules has further been shown to occur in gas bubbles (13), and it has been hypothesized that liposomes may have formed from lipids delivered by meteorites (14). Mineral membranes have been demonstrated to form under putative conditions of the earlier Earth, either in alkaline environments linked to serpentinization (15), in soda lakes (16), or in hydrothermal vents (17). Typically, the abiotic synthesis of the molecular building blocks of life and the formation of vesicles that facilitate reactions toward complexity have been considered two events, separate either in time, space, or both.

Since the pioneering Miller–Urey experiment and subsequent related investigations, it has been well known that lightning or UV irradiation of an inorganic reducing atmosphere synthesizes the molecular bricks of life, such as amino acids and nucleobases, along with solid organic particles (18–20). Recent investigation has shown that the solid organic material and the most relevant prebiotic molecules only form when the reaction is catalyzed by the silicate-rich surfaces of a borosilicate reactor (21). For many years after the Miller experiment, the Hadean eon was considered a dry, very hot wasteland where life had zero probability of emerging. Thus, the common scientific paradigm has been that life must have developed

Author contributions: C.J. and J.M.G.-R. designed research; C.J., A.M.-S., and F.R. performed research; C.J., F.R., L.G.-S., and J.M.G.-R. contributed new reagents/analytic tools; C.J., F.R. and J.M.G.-R. analyzed data; and C.J. and J.M.G.-R. wrote the paper.

The authors declare no competing interest.

This article is a PNAS Direct Submission.

[1]To whom correspondence may be addressed. Email: juanma.garciaruiz@dipc.org.

This article contains supporting information online at https://www.pnas.org/lookup/suppl/doi:10.1073/pnas.2413816122/-/DCSupplemental.

Published December 30, 2024.

during the Archean, when the atmosphere was mildly reducing, consisting primarily of CO_2, H_2O, and N_2 rather than H_2, CO, CH_4, and NH_3, rendering the original Miller experiment of poor relevance in this context. However, more recent investigations suggest that 4.4 billion years ago, during the early Hadean, liquid water already covered the solid crust of ferric-magnesium silicates, triggering serpentinization on a global scale, probably extending until the Archean (22–25). There is mounting evidence that the atmosphere had noticeable quantities of CO, CH_4, and H_2 (26–28). Lightning linked to volcanic activity and/or high-intensity UV irradiation makes the Miller-type experiment an excellent laboratory simulation of the early Hadean times. In this work, we utilized a Miller-type experiment, to demonstrate the self-assembly of biomimetic vesicular structures within the silica-induced solid organic matter forming in such an environment.

Results

Experiments were performed in borosilicate reactors filled with an initial mixture of reducing gases [200 mbar (NH_3):500 mbar (CH_4):250 mbar (N_2)], 200 mL of water, and connected to a generator that supplies energy to the system in the form of electrical discharging (*Materials and Methods*). Over the course of the two-week experiment, the initially clear and highly basic aqueous phase (pH 11.3 to 11.9), further called the "soup" to honor pioneering workers, obtains a strong yellow-brown color, accompanied by slight turbidity and a drop in alkalinity to a pH of 10.1. In addition, a brownish organic film gradually forms on the walls of the borosilicate reactor over the time of the experiment (Fig. 1*A*). This film covers the reactor walls and covers the water–gas interphase despite steady agitation of the soup (*SI Appendix*, Fig. S1). In additional experiments, presence of CO_2 and a variation in methane to nitrogen to CO_2 ratios in the initial atmosphere appeared to achieve similar results (*SI Appendix*). With a thickness ranging from 150 to 3,000 nm throughout the reactor, the bulk structure of the solid organic film (SOF) is composed of fused 50 to 100 nanometer-sized subunits as highlighted in Fig. 1*B*. We found that the SOF bears different characteristics depending on the location inside the reactor. While the SOF in the upper parts near the electrodes is only slightly humid and much thicker, the SOF in the lower parts of the reactor is thin (typically < 500 nm) and soaked with water due to condensation and capillary action. The SOF formed on the meniscus draws water from the underlying reservoir into the gap between the organic film and the borosilicate reactor walls, as indicated by a thin aqueous layer and the film's high pH values. Field-emission scanning electron microscopy (FE-SEM) reveals that the SOF in this region is decorated with micrometer-sized spherical particles, either directly attached or dispersed on the film (Fig. 1*C*). The formation of the spherical particles appears to be related to the presence of condensed water as suggested by their high occurrence on the SOF nearer the water meniscus and water inclusions (*SI Appendix*, Fig. S2). Energy Dispersive X-ray (EDX) analysis of the spheres reveals that their elemental composition is similar to the organic film, however, contains significant amounts of silicon (Fig. 1*D*). Morphologically the majority of the spheres are smooth and attached to the SOF from which they emerge as Fig. 1*C* highlights. A portion of the spherical particles have collapsed like deflated balloons, suggesting their hollowness (Fig. 1 *E* and *F*). We therefore investigated the spheres' internal structure through Focused Ion Beam (FIB) sectioning and FE-SEM imaging as displayed in Fig. 1 *G*–*J*. Noticeably, the majority of the sectioned spheres are hollow, with variable diameters of the interior hole and a variable thickness of the shell (Fig. 1 *H* and *J*). Occasionally, shrunken versions of once smooth spheres are observed, exhibiting wrinkled surfaces that mimic structures of

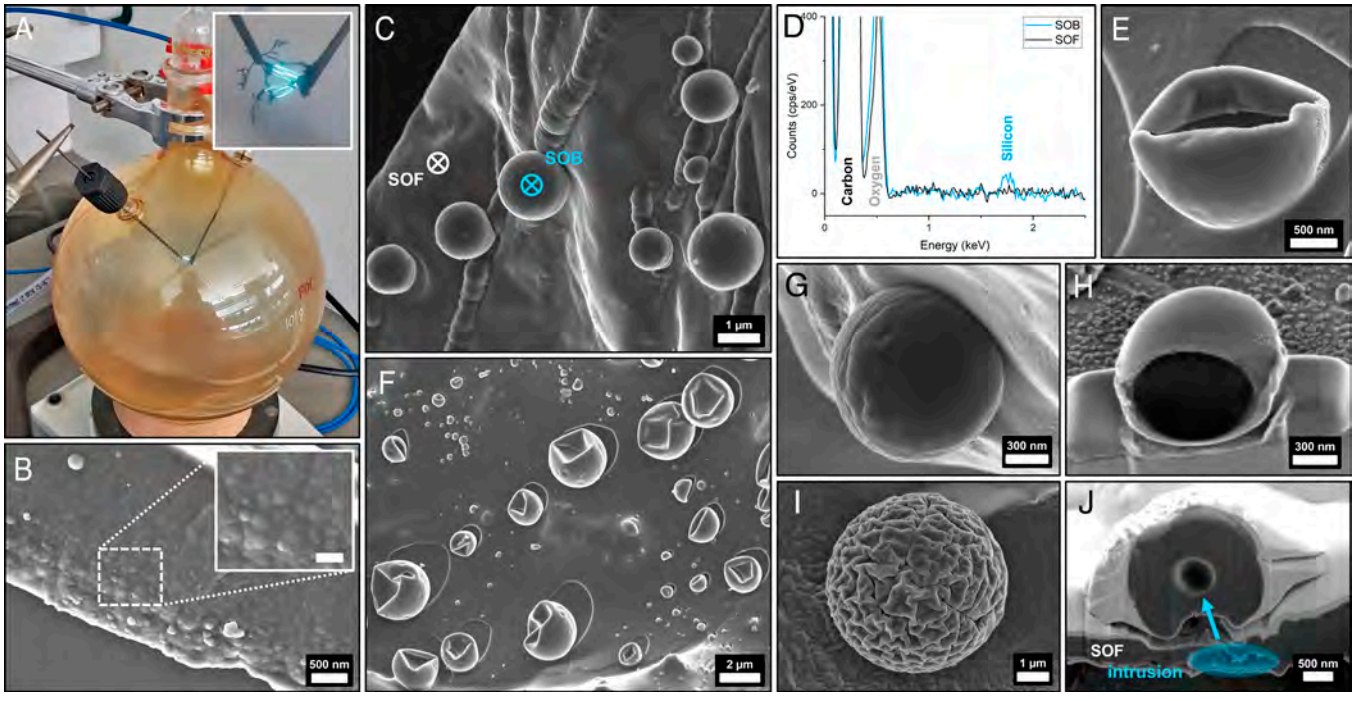

Fig. 1. Vesicular organic biomorphs formed on the SOF. (*A*) shows a photograph of a Miller-type reactor after 7 d of electrical discharging. The FE-SEM micrograph in (*B*) displays a cross-section of the brownish SOF forming on the reactor walls highlighting its bulk structure in the *Inset* (Scale bar is 200 nm.). Image (*C*) shows intact protocells attached to the SOF with the marked locations of corresponding elemental analysis through point EDX (SOF = Solid Organic Film, SOB = Spherical Organic Biomorphs). The EDX spectra in (*D*) indicate an increased content of silicon within the particles (blue spectra) in comparison to the background of the SOF (black spectra) they are sitting on. Micrographs (*E*) and (*F*) display various protocells as they have collapsed, similar to deflated balloons, indicating their hollow internal structure. The inner structure of the particles was analyzed by FIB cross-sectioning of the spheres, with a smooth (*G* and *H*), and a wrinkled (*I* and *J*) shell, revealing that the spherical particles are indeed protocells with varying degrees of hollowness.

biological origin (Fig. 1*I* and *SI Appendix*, Fig. S3). Similar to biological cells, these hollow structures also compartmentalize space, containing liquids, gases, and prebiotic molecules, which is why we further refer to them as protocells.

Apart from the described spherical particles, we found a plethora of other, fascinating organic biomorphs (Fig. 2) ranging from a few hundred nanometers up to several micrometers in size. These are primarily located on the SOF floating on the water reservoir from which they hang into the soup. EDX analysis shows that contain slightly increased amounts of silicon contrary to the SOF they are attached to (*SI Appendix*, Fig. S4). The organic biomorphs can be categorized into three groups based on their morphology. In addition to the "*spherical*" morphologies (Fig. 1) already described above, we found "*caterpillar-like*" morphologies (Fig. 2 *A*–*C*), as well as "*polyp-like*" morphologies (Fig. 2*D*). Cross-section FE-SEM images of these structures performed with FIB reveal their hollow inner structure, as illustrated in Fig. 2*E*. The thinner ends of the caterpillar- and polyp-like biomorphs are always connected to a hollow opening in the organic film from which they are hanging, as shown in Fig. 2 *A* and *E* and *SI Appendix*, Fig. S4. These small openings presumably feed the growth of the biomorphs through a flow of precursors that are directly related to their formation. From this attachment point, the biomorphs appear to grow into the aqueous phase of the soup. Some of the larger polyp-like biomorphs have a small opening at the tip that might act as a vent for escaping gases or liquids (Fig. 2*D*).

Chemical Characterization of the Organic Film and Organic Biomorphs. To understand the chemical nature of the solid organic film, we have performed comparative experiments in the presence and absence of water. We found that the SOF on the reactor walls only forms in the presence of water, in contrast to the sticky, dark-brown oil that forms in the water-free experiments (*SI Appendix*, Fig. S1*E*). These findings are supported by five key observations made through FT-IR analysis and comparing the water-free and standard experiments.

First, FT-IR spectra of the water-free experiment highlight the presence of various α-aminonitriles (Fig. 3*A*). The basic units forming the dark brown oil are hydrogen cyanide analogs, acetonitrile, and other isonitriles, which can polymerize to some extent. Corresponding stretching vibrations of the functional groups C≡N, C=N, CH, and NH can also be identified in the spectra (*SI Appendix*, Table S1 for detailed assignation). In the comparative spectra of the SOF forming in the presence of water these characteristic C≡N stretching vibrations of the brown oil practically disappear as Fig. 3*A* displays. This is in good agreement with previous observations highlighting the conversion of HCN into progressed ladder polymers and oxygenated chains in the presence of H_2O (29).

Second, two characteristic bands observed at 2,188 cm^{-1} and 1,610 cm^{-1} are assigned to the C≡N and N=C stretching vibrations, respectively, only appear in the water-free experiment, assuming hydrogen cyanide dimer and a few longer oligomers are the basic structures (additional discussion is provided in *SI Appendix*).

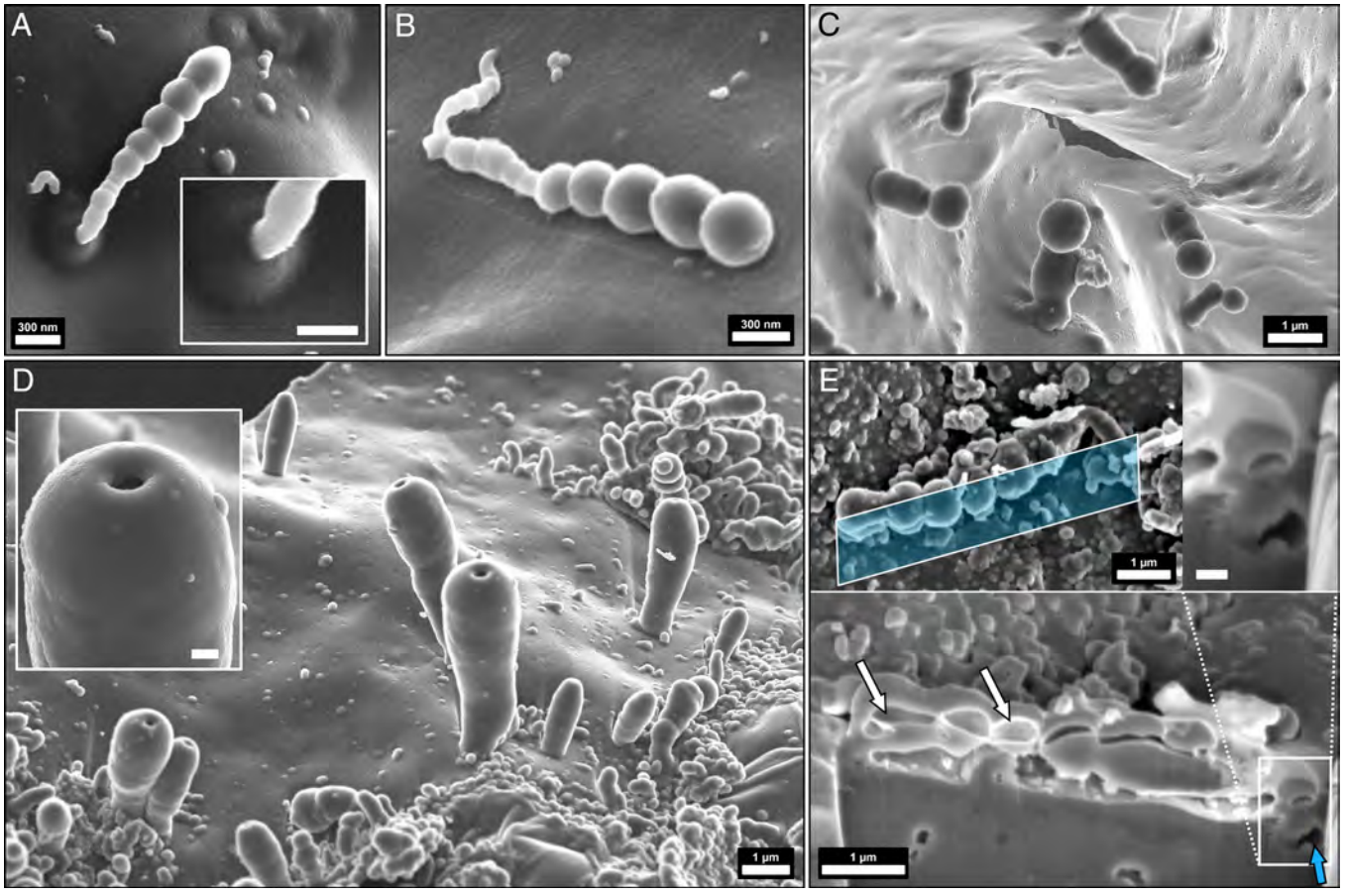

Fig. 2. Organic biomorphs hanging on the SOF. FE-SEM micrographs of caterpillar-like (*A*–*C*) as well as polyp-like (*D*) organic biomorphs. All these structures, which are shown for clarity upside down, are hanging from the SOF into the aqueous reservoir. Note that the thinner ends of these structures are connected to the SOF as the *Inset* in (*A*) highlights. The *Inset* in (*D*) shows a small opening on the terminal ends of the polyp-like structures. A FIB cross-sectioning performed alongside the growth direction of a caterpillar-like biomorph is indicated in blue in image (*E*), revealing its hollow, inner structure (white arrows). The FIB cross-section (removed material indicated by the blue shaded area) further shows the opening inside the SOF where the biomorphs are connected, possibly allowing a flow of precursors responsible for its growth, as indicated by the blue arrow. The scale bar in *Insets* is 200 nm.

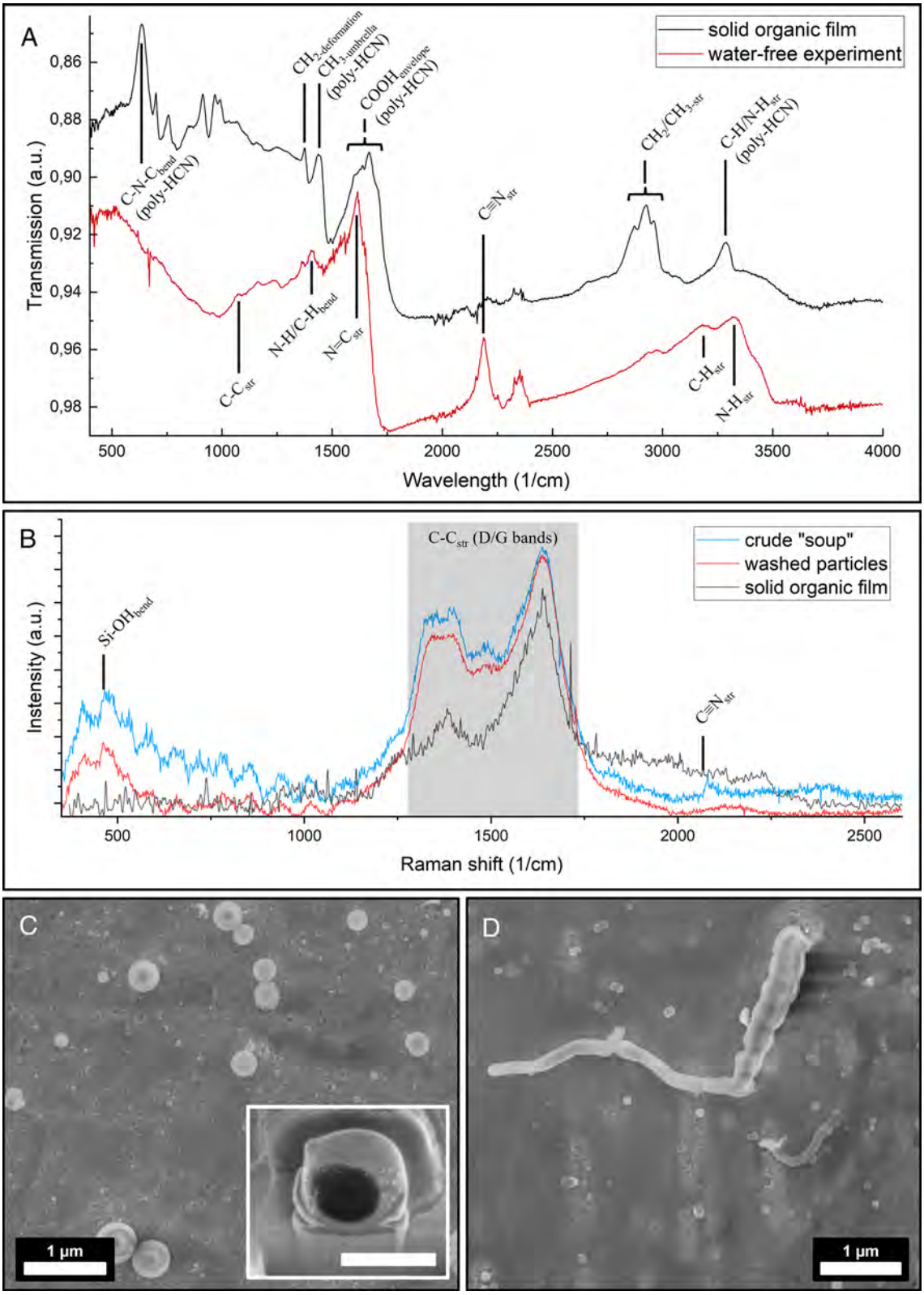

Fig. 3. Spectroscopic analysis of the SOF and the dispersed solid compounds in the soup. Graph (*A*) displays FT-IR spectra of the SOF, and the dark-brown oil obtained in the water-free experiments (*SI Appendix*, Fig. S1*E*). The identified bands, as listed in *SI Appendix*, Table S1, suggest the extensive formation of polymerized HCN in the presence of H_2O which appears to be the primary component of the SOF. In (*B*) Raman spectra are displayed that have been obtained from the dry SOF (black), the dispersed particles in a crude Miller soup (blue), and the washed and redispersed particles in Milli-Q water (red). FE-SEM micrographs in (*C*) and (*D*) display the particles that form a stable dispersion in the soup. After centrifugation and washing, they were transferred onto a copper tape. The *Inset* in (*C*) shows a FIB cross-sectioning performed on a large spherical particle. The scalebar in *Inset* (*C*) is 500 nm.

Third, the C-H stretching bands from CH_2 and CH_3 functional groups with medium-strong intensity and N-H stretching vibrations, which are observed in the dark brown oil, reduce to a single and intense peak at 3,287 cm^{-1} in the SOF. Furthermore, the single band at 1,610 cm^{-1} transforms into a complex envelope containing C=N and C=O vibrations, further suggesting the

polymerization of HCN into a variety of polymers as well as the formation of new molecular species not observed in the water-free experiments.

Fourth, the band at 1,665 cm^{-1} and the shoulder at 1,705 cm^{-1} can be assigned to carboxylic acids in the form of dimers or more complex structures. In combination with the deformation bands at 1,373 cm^{-1} and 1,444 cm^{-1}, that are characteristic of the CH_3 umbrella and CH_2 deformation modes of these species, it is further supporting the polymerization of HCN.

Fifth, in the fingerprint region, several new bands are observed, of which the most important band at 636 cm^{-1} can be associated with the typical bending-modes of a CNC polymeric chain.

In addition, to these observations highlighting the importance of water to these experiments, additional observations were made on the important role of silica. The small features observed at 3,440 cm^{-1} and 1,075 cm^{-1} (both broad), and 473 cm^{-1} can be assigned to the borosilicate OH stretching, Si–O–Si (mixed with BO_3) stretching, and Si–O–Si bending vibrations, respectively. It is noteworthy that the SOF only forms in borosilicate reactors, which can be attributed to the catalytic role of silica in the synthesis of the HCN-polymers, most probably through its silanol groups (21). In addition to FT-IR, we performed Raman spectroscopy on the SOF (Fig. 3*B*), which also shows its polymeric character by the strong D/G bands of the C–C stretching vibrations in the form of a broad doublet at 1,336 cm^{-1} and 1,601 cm^{-1} typically attributed to a polymeric chain.

At the mesoscopic scale, the SOF appears to be primarily composed of nanoparticles that fused to form the bulk of the organic film as described in Fig. 1*B*. Interestingly, we found that nanoparticles of similar size and composition are suspended in the slightly turbid soup. These particles form a stable dispersion as they do not sediment over several weeks (*SI Appendix*, Fig. S5). Dynamic light scattering (DLS) and analytical ultracentrifugation (AUC) experiments reveal that the turbidity indeed stems from nanometer-sized particles with a hydrodynamic diameter of 127.3 ∓ 29.0 nm (FWHM) and a particle density of 1.24 ± 0.04 g/cm which are likely related to the particles composing the SOF (for detailed analysis see Supporting Information). A second particle species, linked to the above-described spherical biomorphs, inhering a broad distribution in size ranging from several hundred to a few thousand nanometers could also be identified floating in the soup as DLS and FE-SEM analysis in Fig. 3 *C* and *D* and *SI Appendix*, Fig. S5 display. Liquid-phase Raman spectroscopy of the dispersed particles illustrated in Fig. 3*B* highlights the chemical similarity to the SOF through the same broad doublet assigned to D/G bands of C–C stretching vibrations of a polymeric chain. Compared to the D/G bands of the SOF, a variation in intensities arises from the absence of carbonaceous particles that typically form around the tungsten electrodes during the 14 d of electrical discharge (*SI Appendix*, Fig. S1*D*). These particles eventually settle on the SOF below, where they become incorporated over time. Very weak bands at 2,180 cm^{-1} and 2,130 cm^{-1} assigned to C≡N stretching vibration are consistent with the IR spectra of the SOF, confirming the polymerization of HCN and the presence of dissolved C≡N species that practically disappear after washing (Fig. 3*B*). The spectra further display strong signals in the region below 500 cm^{-1}. While the peaks at 444 cm^{-1} can be again attributed to the bending modes of the polymer chains, the signal at 465 cm^{-1} is characteristic of Si–O–Si or Si–OH bending vibrations. FE-SEM analysis of the separated particles through centrifugation confirms these observations and demonstrates their morphological similarities to the hollow spherical and worm-like organic biomorphs as displayed in Fig. 3 *C* and *D*. Their hollowness was ultimately confirmed by additional FIB sectioning (Fig. 3 *C*, *Inset*). The fact that silica and polymer signals remain strong after washing the particles in Milli-Q water indicates that silica-rich solution is either trapped inside the hollow biomorphs or silica is part of their composition. We conclude that the solid organic film and the protocells are made of ill-defined poly-HCN nanoparticles formed from the polymerization of HCN, a reaction in which water plays a crucial role (30–32).

Morphogenesis of Organic Biomorphs. The proposed mechanism of morphogenesis of poly-HCN biomorphs is illustrated in Fig. 4. The formation of hydrogen cyanide driven by electrical discharge and UV radiation is well known to convert into formamide (CH_3NO) or directly polymerize into poly-HCN in the presence of water (30–33). In our experiments, atmospheric water vapor promotes the formation of electrically charged nanometer-sized HCN-rich nanodroplets. These droplets deposit on the borosilicate or water interfaces of the reactor, where they fuse and polymerize into a continuous SOF, occasionally encapsulating other organic molecules or liquid droplets, as observed in *SI Appendix*, Fig. S3. The continuous generation of HCN, with its high vapor pressure and low melting point (25.6 °C) as well as the formation of other, gaseous molecules driven by the electrical discharge, slowly increases the pressure inside the reactor by up to 62% from an initial pressure of 793 mbar to 1,283 mbar. After the formation of an initial layer of HCN-polymer, the interaction of HCN and other molecules with water appears to predominantly occur within the porous structures of the SOF. Gaseous byproducts of these reactions, as well as unpolymerized HCN derivates, are concentrated in the SOF, likely leading to the formation of bubbles when they escape into the alkaline soup (Figs. 1*C* and 4*A*). On the newly formed bubble–water interface, the HCN-rich precursors in contact with water will result in the precipitation of poly-HCN, encapsulating the bubble and creating the hollow structures that we observed (Fig. 4 *A*–*C*).

The precipitation rate of this process depends on several factors, like the precursor production rate, the partial pressure of HCN, and the pH of the soup. Therefore, the inhomogeneous local conditions will determine the different morphologies of the observed biomorphs. The formation of a single gas bubble beneath the film (Fig. 4*A*) results in spherical particles that either remain attached to the film or are dislodged by the induced convection and dispersed into the solution (Fig. 4). Low concentrations of HCN and/or low pH slows the precipitation of polymer at the bubble interface. Thus, before full-encapsulation, the intruding precursor molecules may trigger the formation of a secondary bubble (Fig. 2*C*) or, by iteration of this mechanism, the caterpillar-like structures shown in Figs. 2 *A* and *B* and 4*B*. A continuous and steady intrusion of precursor molecules without a full encapsulation will result in the elongated, polyp-like structures (Figs. 2*D* and 4*C*). Whether the poly-HCN skin is permeable, and the protocells are later filled with soup is yet to be confirmed. Nevertheless, the clear silanol signature in the Raman spectra of washed biomorphs (Fig. 3*B*), and their relatively high densities obtained from AUC suggest that they are filled with liquids rather than gas. In both cases, these protocells potentially work as microreactors of relevance for prebiotic chemistry because HCN is considered the source of RNA and protein precursors (34).

Concluding Remarks. Our results suggest that the concomitant formation of poly-HCN microreactors and prebiotic organic molecules induced by silica would turn the waters of early Earth (and any Earth-like planets or moons) into an organic chemistry laboratory at the planetary scale. In this environment, chemical

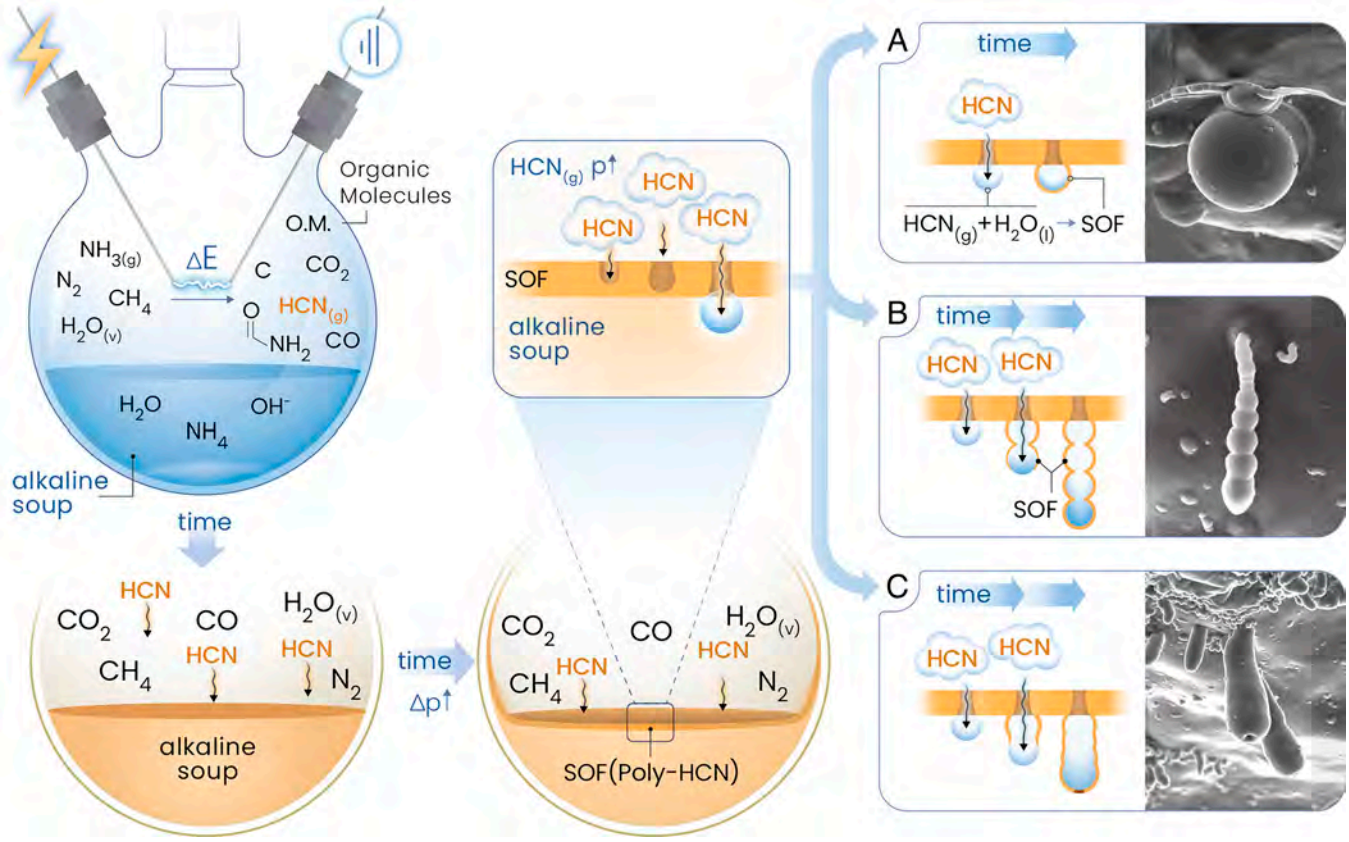

Fig. 4. Mechanistic sketch of the morphogenesis of organic biomorphs. HCN forming inside the Miller reactor reacts with water to form a SOF made of HCN-polymers that cover reactor walls and the water–gas interface of the alkaline soup. The continuous formation of HCN and other HCN derivatives increases the partial pressures and concentration of poly-HCN precursors. Gaseous byproducts of the reaction of these molecules in the porous parts of the SOF lead to the formation of bubbles below the film. (*A*) In contact with the alkaline soup, the HCN polymerizes at the bubble interface forming a thin SOF surrounding the bubble, ultimately resulting in spherical protocells. (*B*) Under specific local conditions, when bubble encapsulation is slow, a continuous flow of precursor molecules results in the formation of a new bubble on the former one. The repetition of this pupping phenomenon is the origin of caterpillar-like biomorphs. (*C*) A slow precipitation of HCN-polymer combined with a steady growth of the bubble allows for elongation, ultimately resulting in polyp-like biomorphs.

complexity can further develop, activated by temperature, UV/photon irradiation, and dry-wet cycles, setting the stage for the emergence of life (29, 33). As discussed by Navrotsky et al., small molecules such as amino acids, oligopeptides, nucleobases, and fatty acids may interact with silica to form functional structures that, in turn, would trigger further polymerization (35). This positive feedback between synthesis and catalysis in silica–organic systems may have created clusters of molecules entrapped into biomorphic microreactors where they can develop into further molecular complexity. Changes in atmospheric composition and variations in the hydrochemistry would trigger different chemical pathways, some of which would eventually lead to the kind of complex, self-sustaining systems we know as life.

In addition, our experimental results call for a reevaluation of life detection studies. The discovery of hollow, biomorphic organic structures resembling streptococci-like morphologies, as shown in Fig. 2, in the oldest Earth or Martian rocks and meteorites—whether alone or in combination with organic molecules such as amino acids and nucleobases—can no longer be regarded as a definitive signature of life. The morphogenetical mechanism of bubble formation followed by the precipitation of an amorphous organic sheath should be added to the discussion on the identification of the proposed remnants of early life forms and dubiofossils (36–40). The bacterial-shaped objects found in meteorites like those in the Martian meteorite Allan Hills 84001 (41), and some of the so-called nanobacteria of controversial origin (42, 43), may also be the results of abiotic mechanisms proposed in this work.

Materials and Methods

Materials. All water used in the experiments was deionized using a Merck Millipore Milli-Q 7003 Water Purification System with a resistance of 18.2 MΩ/cm at 25 °C. All gasses (Nitrogen, Methane, CO_2, and Ammonia) were supplied by Linde in 10-L gas cylinders with purities following the Linde product descriptions: Nitrogen 5.0, Methane 4.5, CO_2 4.5, and Ammonia 3.8. Ground-finished pure tungsten tic welding electrodes with a >99.5% purity according to ISO 6848 were utilized as electrodes.

Miller–Urey Experiments. Prior to the experiment, all glassware was cleaned using a series of chemical baths to first clean the borosilicate glass by soaking it in a saturated potassium hydroxide solution (KOH) in isopropanol for 24 h to remove any containments and impurities off the borosilicate glass surface. Following, the thus hydrolyzed glass surface was restored by subsequent soaking in a 2 M hydrochloric acid, water, bath for another 24 h. The so renewed borosilicate glass was then rinsed with deionized Milli-Q water and sterilized in absolute ethanol (EtOH) for several hours before assembling the tungsten electrodes and connecting the reactor to the gas introduction manifold setup. All other parts of the setup were also cleaned thoroughly with absolute ethanol and a silicon-free high-vacuum grease was applied to seal all connections within the manifold air tight. The custom design of the reactor allows for the adjustment of the length of the tungsten electrodes so that the distance of the tip of the electrodes, where electrical discharging is occurring, can be adjusted to be exactly 10 mm apart.

In the 3 L borosilicate round flask equipped with the two tungsten electrodes, 200 mL of Milli-Q water and a magnetic stir bar were placed. The water was degassed in three cycles to remove any remaining dissolved oxygen. In the first step, ammonia gas was quickly introduced into the reactor to obtain a partial pressure of 200 mbar NH_3. The ammonia was allowed to dissolve into the water

for 15 min before first methane (500 mbar) and then nitrogen (250 mbar) gas was subsequently introduced, and the reactor closed. In comparative experiments, the gas mixture was adjusted to either replace or lower CH_4 and N_2 partial pressures through the addition of CO_2 (*SI Appendix*). Electrical discharging at 35 kV ± 3 kV and a 1 mA current was started between the 10 mm distanced tungsten electrodes inside the reactor with a 15-min on/off cycle for 14 d while continuously stirring at 250 rpm. pH and pressure readings were taken before and after the experiment. During the experiment, the containments of the reactor gained a brownish color, and an organic film formed slowly on the glass and water interfaces. Various solid and liquid samples of different locations inside the reactor were taken and analyzed by FE-SEM, LM, FT-IR, Raman, and AUC analytical techniques. Chemical analysis of the organic compounds formed inside the Miller-type experiments using gas-chromatography coupled with mass spectrometry has already been performed in our previous research (21).

Raman and Infrared Spectroscopy. IR spectra were obtained on a Perkin Elmer Spectrum 100 FT-IR. Universal ATR Sampling Accessory with a spectral resolution of 4 cm^{-1} and 16/32 accumulations. For Raman spectra, a KOSI HoloSpec f/1.8i Raman spectrometer illuminated with a 633 nm: Laser REO LSRP-3501 and a CCD detector Andor DV420A-OE-130 was used. The observation was made with a Nikon Eclipse E600 microscope coupled to a KOSI HFPH-FC-S-632.8 Raman head. Experimental conditions: 100× LF objective, 0,8 mW laser power on the sample to avoid thermal perturbation of the samples, and 6 cm^{-1} spectral resolution. Spectra were corrected by the instrumental spectral response and baseline.

FE-SEM and EDX Spectroscopy. FE-SEM of the SOF has been performed on an AURIGA from Carl Zeiss SMT using an acceleration voltage of 3 kV. Before measurement, the samples have been sputtered with a 10 to 20 nm thin coating of elemental carbon. Extended analytics regarding elemental composition through EDX have been conducted on the equipped Oxford Instruments INCAx-act (PentaFET precision) detector of this instrument.

FIB Analysis. Cross-sectioning of the SOF and the organic biomorphs was performed using a Thermo Fischer Scios 2 DualBeam microscope, combining an HR-SEM and a FIB column. The microscope is equipped with a precursor-based gas injection system allowing for high-precision cuts in the submicrometer range. The surface of the samples objected to cross-sectioning are protected from altering using a platinum coating process before applying the gallium-ion beam with a varying emission current of 1 to 5 nA at a 30 kV acceleration voltage. For high-precision cuts, the beam current was lowered to 50 to 100 pA. HR-SEM images were recorded using the Trinity Detection System (in-lens and in-column) with T1 segmented lower in-lens detector and T2 upper in-lens detector. In addition, the Everhart–Thornley secondary electron Detector has been used.

AUC. The AUC measurements were performed on an Optima XL-A (Beckman Coulter, Palo Alto, CA) using absorbance (OR Rayleigh interference) optics at 20 °C at 2,000 rpm for H_2O and 5,000 rpm for D_2O respectively. 20 mm double-sector titanium centerpieces (Nanolytics, Potsdam, Germany) were used for all experiments. The filled rotor with the cells was tempered to 20 °C for 1 h before the start of each experiment. Sedfit [version 16.1c by Peter Schuck (44)] was used for performing the g(s) distributions with the ls-g*(s) model and Tikhonov–Phillips regularization (45). The final fitted densities from the solvent variation experiment were used for the calculations of the hydrodynamic diameter of particles.

Data, Materials, and Software Availability. All study data are included in the article and/or *SI Appendix*.

ACKNOWLEDGMENTS. We thank A. González Segura for her help in the FE-SEM and EDX measurements, and all the staff at the Centro de Instrumentación Científica at the University of Granada for their assistance. We like to acknowledge Prof. Mark van Zuilen, Prof. Wolfgang Bach, Dr. Bruno Bizarri, Prof. Raffaele Saladino, Prof. José María Asua, and Professor Fernando Cossío, and Dr. Fermín Otálora for their useful discussions. We further want to acknowledge the assistance of Dr. Luis Gonzalez-Ramirez and the members of the Laboratorio de Estudios Cristalográficos at the Instituto Andaluz de Ciencias de la Tierra. We further want to thank Dirk Haffke and Rose Rosenberg for their support and expertise in conducting AUC measurements in the working group of Prof. Helmut Cölfen at the University of Konstanz. We want to thank Guillermo Lopez-Reyes and Aurelio Sanz from the University of Valladolid (Project PID2022-142490OB-C32) for contributing to the Raman study.

Author affiliations: [a]Laboratory of Crystallographic Studies, Instituto Andaluz de Ciencias de la Tierra, Consejo Superior de Investigaciones Científica, Armilla 18100, Spain; [b]Espectroscopía Raman e Infrarroja aplicado a Cosmogeoquímica y Astrobiología Research Group, Department of Applied Physics, Universidad de Valladolid, Boecillo 47151, Spain; [c]División de Microscopía Electrónica, Servicios Centrales de Investigación Científica y Tecnológica, Universidad de Cádiz, Cádiz 11519, Spain; and [d]Donostia International Physics Center, Donostia/San Sebastián 20018, Spain

1. D. E. Koshland, The seven pillars of life. *Science* **295**, 2215–2216 (2002).
2. F. M. Harold, F. M. Harold, *The Way of the Cell: Molecules, Organisms, and the Order of Life* (Oxford University Press, 2003).
3. S. Mukherjee, *The Song of the Cell: An Exploration of Medicine and the New Human* (Simon and Schuster, 2022).
4. B. Drobot *et al.*, Compartmentalised RNA catalysis in membrane-free coacervate protocells. *Nat. Commun.* **9**, 3643 (2018).
5. P.-A. Monnard, D. W. Deamer, Membrane self-assembly processes: Steps toward the first cellular life. *Anat. Rec.* **268**, 196–207 (2002).
6. G. Piedrafita, P.-A. Monnard, F. Mavelli, K. Ruiz-Mirazo, Permeability-driven selection in a semi-empirical protocell model: The roots of prebiotic systems evolution. *Sci. Rep.* **7**, 3141 (2017).
7. J. Lombard, P. López-García, D. Moreira, The early evolution of lipid membranes and the three domains of life. *Nat. Rev. Microbiol.* **10**, 507–515 (2012).
8. E. J. Javaux, Challenges in evidencing the earliest traces of life. *Nature* **572**, 451–460 (2019).
9. R. Buick, Microfossil recognition in Archean rocks: An appraisal of spheroids and filaments from a 3500 M.Y. old chert-barite unit at North Pole, Western Australia. *PALAIOS* **5**, 441–459 (1990).
10. J. L. Vago *et al.*, Habitability on early Mars and the search for biosignatures with the ExoMars Rover. *Astrobiology* **17**, 471–510 (2017).
11. S. F. Jordan *et al.*, Promotion of protocell self-assembly from mixed amphiphiles at the origin of life. *Nat. Ecol. Evol.* **3**, 1705–1714 (2019).
12. W. R. Hargreaves, D. W. Deamer, Liposomes from ionic, single-chain amphiphiles. *Biochemistry* **17**, 3759–3768 (1978).
13. M. Morasch *et al.*, Heated gas bubbles enrich, crystallize, dry, phosphorylate and encapsulate prebiotic molecules. *Nat. Chem.* **11**, 779–788 (2019).
14. W. Gilbert, Origin of life: The RNA world. *Nature* **319**, 618–618 (1986).
15. J. M. García-Ruiz, E. Nakouzi, E. Kotopoulou, L. Tamborrino, O. Steinbock, Biomimetic mineral self-organization from silica-rich spring waters. *Sci. Adv.* **3**, e1602285 (2017).
16. M. Getenet, J. M. García-Ruiz, C. Verdugo-Escamilla, I. Guerra-Tschuschke, Mineral vesicles and chemical gardens from carbonate-rich alkaline brines of Lake Magadi, Kenya. *Crystals* **10**, 467 (2020).
17. M. J. Russell, R. M. Daniel, A. J. Hall, J. A. Sherringham, A hydrothermally precipitated catalytic iron sulphide membrane as a first step toward life. *J. Mol. Evol.* **39**, 231–243 (1994).
18. S. L. Miller, A production of amino acids under possible primitive Earth conditions. *Science* **117**, 528–529 (1953).
19. J. L. Bada, A. Lazcano, Prebiotic soup–revisiting the Miller experiment. *Science* **300**, 745–746 (2003).
20. A. P. Johnson *et al.*, The Miller volcanic spark discharge experiment. *Science* **322**, 404–404 (2008).
21. J. Criado-Reyes, B. M. Bizzarri, J. M. García-Ruiz, R. Saladino, E. Di Mauro, The role of borosilicate glass in Miller-Urey experiment. *Sci. Rep.* **11**, 21009 (2021).
22. P. L. Clay *et al.*, Extreme serpentinization and desulfurization in an early Earth setting. *Geology* **51**, 602–606 (2023).
23. Y. Miyazaki, J. Korenaga, A wet heterogeneous mantle creates a habitable world in the Hadean. *Nature* **603**, 86–90 (2022).
24. J. M. García-Ruiz, M. A. van Zuilen, W. Bach, Mineral self-organization on a lifeless planet. *Phys. Life Rev.* **34–35**, 62–82 (2020).
25. R. Tamblyn, J. Hermann, Geological evidence for high H2 production from komatiites in the Archaean. *Nat. Geosci.* **16**, 1194–1199 (2023).
26. K. J. Zahnle, M. Gacesa, D. C. Catling, Strange messenger: A new history of hydrogen on Earth, as told by Xenon. *Geochim. Cosmochim. Acta* **244**, 56–85 (2019).
27. K. J. Zahnle, R. Lupu, D. C. Catling, N. Wogan, Creation and evolution of impact-generated reduced atmospheres of early Earth. *Planet. Sci. J.* **1**, 11 (2020).
28. J. M. García-Ruiz, M. A. van Zuilen, W. Bach, Mineral self-organization on a lifeless planet. *Phys. Life Rev.* **34–35**, 62–82 (2020).
29. C. N. Matthews, R. D. Minard, Hydrogen cyanide polymers, comets and the origin of life. *Faraday Discuss.* **133**, 393–401 (2006).
30. R. Stribling, S. L. Miller, Energy yields for hydrogen cyanide and formaldehyde syntheses: The HCN and amino acid concentrations in the primitive ocean. *Orig. Life Evol. Biosph.* **17**, 261–273 (1987).
31. J. P. Ferris, W. J. Hagan, HCN and chemical evolution: The possible role of cyano compounds in prebiotic synthesis. *Tetrahedron* **40**, 1093–1120 (1984).
32. M. Ruiz-Bermejo, J. L. de la Fuente, C. Pérez-Fernández, E. Mateo-Martí, A comprehensive review of HCN-derived polymers. *Processes* **9**, 597 (2021).
33. A. M. Saitta, F. Saija, Miller experiments in atomistic computer simulations. *Proc. Natl. Acad. Sci. U.S.A.* **111**, 13768–13773 (2014).
34. T. Das, S. Ghule, K. Vanka, Insights into the origin of life: Did it begin from HCN and H2O? *ACS Cent. Sci.* **5**, 1532–1540 (2019).
35. A. Navrotsky *et al.*, Cooperative formation of porous silica and peptides on the prebiotic Earth. *Proc. Natl. Acad. Sci. U.S.A.* **118**, e2021117118 (2021).

36. J. W. Schopf, Microfossils of the early Archean Apex Chert: New evidence of the antiquity of life. *Science* **260**, 640–646 (1993).
37. A. Lepland, M. A. van Zuilen, G. Arrhenius, M. J. Whitehouse, C. M. Fedo, Questioning the evidence for Earth's earliest life–Akilia revisited. *Geology* **33**, 77–79 (2005).
38. M. A. van Zuilen, A. Lepland, G. Arrhenius, Reassessing the evidence for the earliest traces of life. *Nature* **418**, 627–630 (2002).
39. J. M. García-Ruiz *et al.*, Self-assembled silica-carbonate structures and detection of ancient microfossils. *Science* **302**, 1194–1197 (2003).
40. J. Rouillard, M. van Zuilen, C. Pisapia, J.-M. Garcia-Ruiz, An alternative approach for assessing biogenicity. *Astrobiology* **21**, 151–164 (2021).
41. D. S. McKay *et al.*, Search for past life on Mars: Possible relic biogenic activity in Martian meteorite ALH84001. *Science* **273**, 924–930 (1996).
42. P. J. R. Uwins, R. I. Webb, A. P. Taylor, Novel nano-organisms from Australian sandstones. *Am. Mineral.* **83**, 1541–1550 (1998).
43. C.-Y. Wu, L. Young, D. Young, J. Martel, J. D. Young, Bions: A family of biomimetic mineralo-organic complexes derived from biological fluids. *PLoS One* **8**, e75501 (2013).
44. P. Schuck, P. Rossmanith, Determination of the sedimentation coefficient distribution by least-squares boundary modeling. *Biopolymers* **54**, 328–341 (2000).
45. P. H. Brown, P. Schuck, Macromolecular size-and-shape distributions by sedimentation velocity analytical ultracentrifugation. *Biophys. J.* **90**, 4651–4661 (2006).